





# Directly photoexcited Dirac and Weyl fermions in ZrSiS and NbAs

Cite as: Appl. Phys. Lett. **113**, 221906 (2018); <https://doi.org/10.1063/1.5055207>

Submitted: 06 September 2018 . Accepted: 09 November 2018 . Published Online: 28 November 2018

Chris P. Weber , Leslie M. Schoop , Stuart S. P. Parkin , Robert C. Newby, Alex Nateprov, Bettina Lotsch, Bala Murali Krishna Mariserla, J. Matthew Kim, Keshav M. Dani , Hans A. Bechtel, Ernest Arushanov, and Mazhar Ali



View Online



Export Citation



CrossMark

## ARTICLES YOU MAY BE INTERESTED IN

[Similar ultrafast dynamics of several dissimilar Dirac and Weyl semimetals](#)

Journal of Applied Physics **122**, 223102 (2017); <https://doi.org/10.1063/1.5006934>

[Anomalous Hall effect in polycrystalline Mn<sub>3</sub>Sn thin films](#)

Applied Physics Letters **113**, 222405 (2018); <https://doi.org/10.1063/1.5051495>

[Anomalous Hall effect in thin films of the Weyl antiferromagnet Mn<sub>3</sub>Sn](#)

Applied Physics Letters **113**, 202402 (2018); <https://doi.org/10.1063/1.5064697>

## Lock-in Amplifiers up to 600 MHz

starting at

\$6,210



 Zurich Instruments

Watch the Video 

## Directly photoexcited Dirac and Weyl fermions in ZrSiS and NbAs

Chris P. Weber,<sup>1,a)</sup> Leslie M. Schoop,<sup>2</sup> Stuart S. P. Parkin,<sup>3</sup> Robert C. Newby,<sup>1</sup>  
 Alex Nateprov,<sup>4</sup> Bettina Lotsch,<sup>5,6</sup> Bala Murali Krishna Mariserla,<sup>7,8</sup> J. Matthew Kim,<sup>1</sup>  
 Keshav M. Dani,<sup>7</sup> Hans A. Bechtel,<sup>9</sup> Ernest Arushanov,<sup>4</sup> and Mazhar Ali<sup>3</sup>

<sup>1</sup>*Department of Physics, Santa Clara University, 500 El Camino Real, Santa Clara, California 95053-0315, USA*

<sup>2</sup>*Department of Chemistry, Princeton University, Princeton, New Jersey 08544, USA*

<sup>3</sup>*Max Planck Institute of Microstructure Physics, Weinberg 2, 06120 Halle, Germany*

<sup>4</sup>*Institute of Applied Physics, Academy of Sciences of Moldova, Academiei Str. 5, MD 2028 Chisinau, Moldova*

<sup>5</sup>*Max Planck Institute for Solid State Research, Heisenbergstrasse 1, 70569 Stuttgart, Germany*

<sup>6</sup>*Department of Chemistry, Ludwig-Maximilians-Universität München, Butenandtstrasse 5-13, 81377 München, Germany*

<sup>7</sup>*Femtosecond Spectroscopy Unit, Okinawa Institute of Science and Technology Graduate University, 1919-1 Tancha, Onna-son, Kunigami, Okinawa 904-0495, Japan*

<sup>8</sup>*School of Physical Sciences, Central University of Karnataka, Kadaganchi 585367, India*

<sup>9</sup>*Advanced Light Source Division, Lawrence Berkeley National Laboratory, Berkeley, California 94720, USA*

(Received 6 September 2018; accepted 9 November 2018; published online 28 November 2018)

We report ultrafast optical measurements of the Dirac line-node semimetal ZrSiS and the Weyl semimetal NbAs, using mid-infrared pump photons from 86 meV to 500 meV to directly excite Dirac and Weyl fermions within the linearly dispersing bands. In NbAs, the photoexcited Weyl fermions initially form a non-thermal distribution, signified by a brief spike in the differential reflectivity whose sign is controlled by the relative energy of the pump and probe photons. In ZrSiS, electron-electron scattering rapidly thermalizes the electrons, and the spike is not observed. Subsequently, hot carriers in both materials cool within a few picoseconds. This cooling, as seen in the two materials' differential reflectivity, differs in sign, shape, and timescale. Nonetheless, we find that it may be described in a simple model of thermal electrons, without free parameters. The electronic cooling in ZrSiS is particularly fast, which may make the material useful for optoelectronic applications. *Published by AIP Publishing.*

<https://doi.org/10.1063/1.5055207>

Interest has surged recently in topological semimetals whose low-energy excitations are Dirac or Weyl fermions.<sup>1-4</sup> These materials' technological potential is enhanced by exotic optical effects, predicted<sup>5-10</sup> and observed,<sup>11</sup> including giant second-harmonic generation in the infrared. They have been used to make broadband infrared photodetectors<sup>12-15</sup> whose response time can be just a few picoseconds,<sup>12</sup> and a passive optical switch for picosecond mode-locking of a mid-infrared laser.<sup>16</sup> Such applications call for deeper understanding of the materials' ultrafast optical properties.

The ultrafast dynamics of the 3D topological semimetals are broadly similar to each other,<sup>17</sup> and typically consist of two parts. The first part, a sub-picosecond spike, is sometimes ascribed to the thermalization process by which the initial, photoexcited distribution of electrons evolves into a Fermi-Dirac distribution,<sup>17,18</sup> or alternately ascribed to the cooling of hot electrons by optical phonons.<sup>19-23</sup> The spike has not been observed when the pump and probe photons have different energies.<sup>18,24</sup> The second, slower part of the ultrafast response typically decays in a few picoseconds, matching the response time of Cd<sub>3</sub>As<sub>2</sub>-based devices.<sup>12,16</sup> There is growing evidence<sup>18,20-22,24</sup> that this slow decay represents the cooling of electrons and holes whose temperature exceeds that of the lattice, so that the electronic cooling rate appears to determine the speed of devices made from topological semimetals.

Though the linear electronic dispersion of Dirac and Weyl semimetals resembles graphene's, the Dirac (or Weyl) fermions in these materials exist over a smaller range of energies extending into the mid-infrared. To study the Dirac fermions' dynamics, ultrafast experiments have typically photoexcited electrons and holes with 1.5-eV photons, well beyond the topological bands. Some of these carriers then relax into the topological bands, where they may be observed by an infrared probe<sup>18,24,25</sup> or by photoemission;<sup>21,22,26</sup> other carriers relax without passing through the topological bands,<sup>26</sup> and are not measured. Though it is preferable to directly excite Dirac carriers by a mid-infrared pulse, very few experiments have explored their dynamics.<sup>18,25</sup>

In this work, we use photons from 86 meV to 500 meV to directly excite Dirac and Weyl fermions in ZrSiS and NbAs, and we measure  $\Delta R(t)$ , the change in reflectivity of a time-delayed mid-infrared probe pulse. ZrSiS is a Dirac line-node semimetal<sup>27</sup> with a Fermi energy<sup>28</sup>  $E_F = 13$  meV, while NbAs is a Weyl semimetal<sup>29</sup> with  $E_F = -125$  meV.<sup>30,31</sup> We find that the two materials' ultrafast responses differ radically in shape, sign, and timescale. Nonetheless, in both materials,  $\Delta R(t)$  features a prominent component owing to the cooling of photoexcited carriers by phonons, and a single, simple model of thermal electrons unifies the materials' diverse responses. Additionally, in NbAs, we observe a sub-picosecond spike, whose sign is controlled by the energy of the pump photons. This spike signifies directly excited Weyl fermions, and it decays as they thermalize. However, in

<sup>a)</sup>Electronic mail: cweber@scu.edu

ZrSiS, the data shows no initial spike. We attribute this difference to the line node's much greater density of states, which allows thermalization to proceed so rapidly that, within our time resolution, a nonthermal distribution never occurs. The component representing electronic cooling can have a decay rate as fast as  $\gamma = 5 \text{ ps}^{-1}$ , suggesting that ZrSiS may be particularly well-suited for fast optical devices.

Figure 1 illustrates the scheme of the measurement. Both the pump and the probe energies lie within, or nearly within, the linear dispersion. Transitions above  $2E_F$  result in interband absorption and directly excite Dirac or Weyl fermions. Those below  $2E_F$  are Pauli-blocked (though incompletely so at room temperature), and energy is absorbed primarily through Drude heating. The energies used give us access to both regimes in NbAs, and just to the interband regime in ZrSiS. NbAs has the added complication that non-topological bands intersect  $E_F$ ,<sup>30,31</sup> allowing intraband transitions even at low energy. However, the conductivity is dominated by the Weyl carriers,<sup>30</sup> as happens in other topological semimetals.<sup>32,33</sup> Our results for NbAs will be well described by considering only the Weyl bands, though we cannot exclude some additional effect from the non-topological bands.

Our two-color, transient pump-probe measurements employed a reflection geometry using 1 kHz, 800 nm, 70 fs amplified laser pulses with 5 mJ of energy. We derived pump and probe wavelengths separately from two optical parametric amplifiers (OPAs) which were pumped with 4 mJ and 1 mJ, respectively. The OPAs were capable of generating mid-IR wavelengths from  $2.6 \mu\text{m}$  to  $22 \mu\text{m}$  by difference frequency generation. The resulting time resolution was about 100 fs. The pump fluence was typically about  $10 \text{ mJ/cm}^2$ , enough to strongly saturate the absorption, which improves the spatial homogeneity of the excited region. (See the [supplementary material](#) for further details.) Measurements were done at room temperature.

Single crystals of ZrSiS were grown *via* iodine vapor transport, following the method of Ref. 27. NbAs single crystals with dimensions of a few millimeters and well-faceted surfaces were grown by vapor transport with iodine. We combined crystal growth with synthesis in sealed quartz ampoules. Crystals grew at  $850^\circ\text{C}$  in the center, with arsenic at  $610^\circ\text{C}$  on one side and niobium foil at  $800^\circ\text{C}$  on the other. X-ray diffraction confirmed the NbAs phase. The surface of the NbAs sample was polished with 20-nm paper for flatness. In pump-probe experiments at 1.5 eV, such

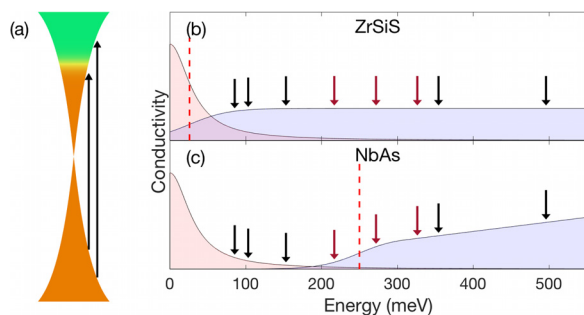


FIG. 1. (a) Representation of the photoexcitation process for photon energies below or above  $2E_F$ . (b) and (c) Schematic representation of the real conductivity, with Drude (red) and interband (blue) contributions. The dashed lines are  $2E_F$ . The black (red) arrows are pump (probe) energies.

polishing is known to suppress bulk-to-surface scattering and thereby eliminate a 50-fs transient.<sup>23</sup>

The differences between ZrSiS and NbAs are immediately apparent in Fig. 2, which shows the results of our pump-probe measurements for several choices of the pump and probe wavelengths. For ZrSiS,  $\Delta R$  is always positive, rises abruptly, and decays swiftly. The measured decay is entirely independent of the probe wavelength (not shown), and it depends weakly on the pump wavelength, with the decay rate  $\gamma$  slowing from about  $5 \text{ ps}^{-1}$  to  $2.5 \text{ ps}^{-1}$  as the pump-photon energy is raised. The ultrafast response of NbAs is more complicated.  $\Delta R(t)$  begins with a sub-picosecond spike, which may be either positive or negative.  $\Delta R(t)$  subsequently becomes negative, gradually reaching a minimum value in about a picosecond, then decaying toward zero during the next few picoseconds. This basic shape experiences several variations as the pump wavelength is changed. For low-energy pump photons, the initial spike is small and negative, and the subsequent, slower decay begins at a fairly negative  $\Delta R$ . For high-energy pump photons, the initial spike is large and positive; the slower decay begins near  $\Delta R = 0$  and takes longer to reach its minimum value. At an intermediate pump energy of 350 meV, the initial spike is first positive and then negative, a behavior it maintains, though less strikingly, when the probe is changed from 270 meV to 220 meV. (This peculiar behavior, and its variation with the probe wavelength, will be discussed further below.)

The diverse behaviors we observe in  $\Delta R(t)$  may appear to require diverse or complicated explanations. We will show, however, that nearly all of our data may be explained by the simple mechanism of phase-space filling—in which the occupation of a state above the node by an electron (or below the

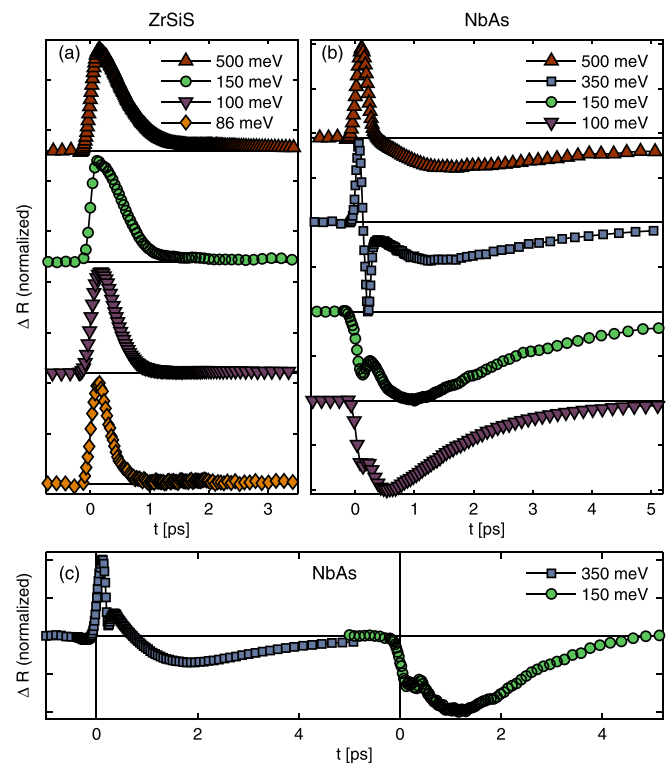


FIG. 2. Pump-probe reflectivity measured at a fixed probe wavelength for a variety of pump-photon energies. The curves are normalized and shifted vertically for clarity. (a) ZrSiS, probed with 270-meV photons. (b) NbAs, probed with 270 meV. (c) NbAs, probed with 220 meV. (Curves shifted horizontally.)

node by a hole) suppresses further optical absorption *via* the Pauli exclusion principle. During the initial spike (occurring in NbAs), the phase space is filled by a nonthermal distribution of photoexcited electrons and holes [Fig. 4(a)]. Subsequently, these carriers thermalize by electron-electron scattering, leaving the Weyl (or Dirac) fermions at an elevated temperature; phase space is filled by thermally excited electrons and holes [Fig. 3(a), inset].

We begin by discussing the latter, thermal behavior, for which we can construct a simple model that agrees quantitatively with our observations. The calculations, which we outline here, are detailed in the [supplementary material](#). We let  $T_e = \Delta T_e + 300$  K be the electrons' instantaneous temperature, with  $\Delta T_e$  being the transient heating above room temperature.  $T_e$  determines a Fermi-Dirac occupation function  $f(T_e)$  with the chemical potential chosen to conserve electron number. We use a simplified density of states:  $g(E) \propto E$  around a line node, and  $g(E) \propto E^2$  around a point node. We determine the change in the real conductivity  $\Delta\sigma_1(\omega)$  through the Kubo-Greenwood formula (Eq. S1 of the [supplementary material](#)), and the change in the imaginary conductivity  $\Delta\sigma_2(\omega)$  through the Kramers-Kronig relations; these determine  $\Delta R(\Delta T_e)$ .

The results of this calculation appear in Fig. 3(a). The key observation is that for ZrSiS  $\Delta R$  is positive for nearly all electronic temperatures, while for NbAs,  $\Delta R$  is non-monotonic, and is negative unless  $\Delta T_e$  exceeds 590 K. The overall magnitude of  $\Delta R$  in these curves is arbitrary. For NbAs, however,  $\Delta R$  reaches a minimum at 250 K, which overcomes the arbitrary vertical scaling: by identifying the minimum measured  $\Delta R$  with the minimum calculated  $\Delta R$ , we can extract  $\Delta T_e(t)$  from the measured  $\Delta R(t)$ . The result of this analysis appears in

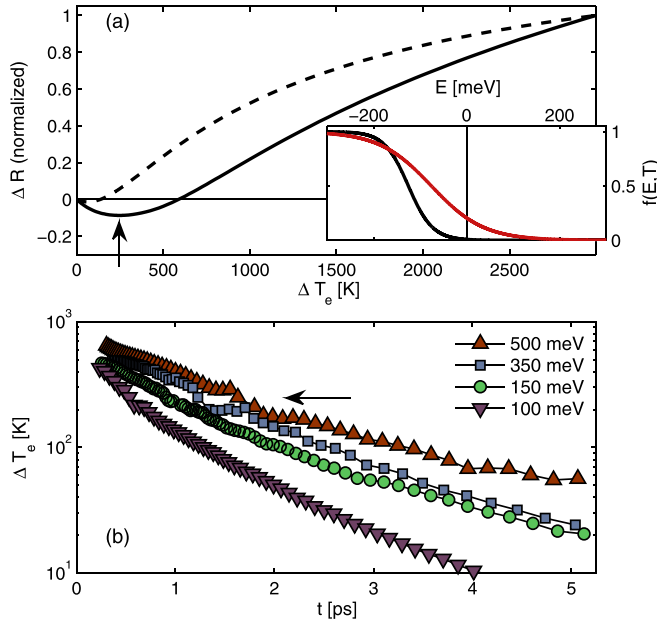


FIG. 3. (a) Simulation of  $\Delta R$  vs.  $\Delta T_e$  for thermal electrons, for a 270-meV probe. The solid line is for NbAs, and the dashed line is for ZrSiS. Inset: examples of the Fermi function for NbAs at 300 K (black) and 1000 K (red). (b) Transient electron temperature of NbAs, as inferred from the measured  $\Delta R(t)$  *via* the curve in panel (a), for several values of the pump-photon energy. The arrows indicate the temperature at which  $\Delta R$  reaches its minimum.  $\Delta T_e(t)$  is similar when probed at 220 meV (see [supplementary material](#)).

Fig. 3(b). The initial electronic temperatures are of order 500 K, and pump photons with higher energy  $E_p$  result in a higher initial  $T_e$ . The electrons cool during the next few picoseconds, and the cooling rate gradually slows, with its instantaneous decay rate  $\gamma$  dropping from about  $1.2$  ps $^{-1}$  to about  $0.35$  ps $^{-1}$ . This slowing is consistent with the well-known phonon bottleneck,<sup>22,34</sup> in which electronic cooling is mediated first by optical phonons, then by acoustic phonons. Our measured rates are much faster than the  $0.08$  ps $^{-1}$  seen in Cd<sub>3</sub>As<sub>2</sub>,<sup>18</sup> but similar to those measured in MoTe<sub>2</sub>,<sup>22</sup> which slowed from  $2.3$  ps $^{-1}$  to  $0.24$  ps $^{-1}$ . Analysis by a two-temperature model (see the [supplementary material](#)) enables us to estimate the electron-phonon coupling in NbAs as  $260$ – $600$  (meV)<sup>2</sup>, much higher than what was measured in MoTe<sub>2</sub>.<sup>22</sup>

For ZrSiS, the calculated  $\Delta R$  [Fig. 2(a)] and the measured ones [Fig. 1(a)] both lack local extrema, so we cannot infer  $\Delta T_e$  from our data. Nonetheless, the calculated  $\Delta R(T_e)$  is concave down, which does explain the most prominent trend in the ZrSiS data, namely that the signal relaxes more slowly for more energetic pump photons. This slowing occurs because a higher  $E_p$  results in a higher initial  $T_e$ , and thus in a lower slope of  $\Delta R$  vs.  $T_e$ . Notably, the decay rate  $\gamma$  of  $5$  ps $^{-1}$  to  $2.5$  ps $^{-1}$  indicates that electrons in ZrSiS cool much faster than in NbAs, or indeed other topological semimetals,<sup>18,21,24</sup> with only WTe<sub>2</sub> and MoTe<sub>2</sub> coming close.<sup>20,22</sup> Such rapid cooling requires a strong electron-phonon interaction, for which Raman studies provide some evidence.<sup>35</sup>

Next, we consider the cause of the rapid positive or negative spike that occurs in NbAs, but not in ZrSiS. Optical coherence between pump and probe pulses can sometimes give rise to a similar spike, but our pump and probe cannot be coherent since they differ in frequency.<sup>36</sup> Even in the absence of coherence, when the pump and probe are simultaneous, a negative spike may arise from two-photon absorption,<sup>36</sup> or a positive one from off-resonant electronic Raman excitation.

However, phase-space filling explains the spike more simply than either of these effects, because it can cause both positive and negative spikes with a single mechanism. The curve of Fig. 3(a) shows that the spike cannot represent phase-space filling by thermal electrons—that would require  $T_e(t)$  to be non-monotonic. Rather, in the brief time before electrons thermalize with each other, the electrons and holes occupy phase space at  $\pm E_p/2$  [Fig. 4(a)], reducing  $\sigma_1$  at this

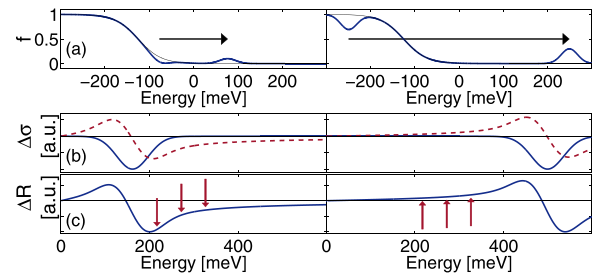


FIG. 4. (a) Nonthermal occupation functions of NbAs, as modeled for pumps of 150 meV (left) and 500 meV (right). The arrow indicates the optical transition made by the pump. Absorption of the lower-energy pump is suppressed by Pauli blocking. The occupation function prior to excitation is shown in the background. (b) The resulting  $\Delta\sigma_1$  (solid) and  $\Delta\sigma_2$  (dashed). (c)  $\Delta R$ . The arrows indicate probe energies used.

energy through phase-space filling, and modifying  $\sigma_2$  [Fig. 4(b)]. The resulting  $\Delta R$  appears in Fig. 4(c). The calculated result agrees with our measurements: when the pump photons are more (less) energetic than the probe,  $\Delta R$  is positive (negative). We observe that the negative peaks are much smaller than the positive ones, which is expected: when  $E_p < 2E_F$ , the Pauli principle suppresses interband absorption, though at finite temperature some absorption can still occur.

This picture may even hint at an explanation for the peculiar behavior observed at a pump energy of 350 meV, where the initial spike is first positive, then negative. Though most of our data are fairly insensitive to changes of the probe energy, this sign change is more pronounced for a 270-meV probe than for 220 meV, which is farther below the pump energy. We suggest that possibly the sign-change may signify the scattering of a portion of the nonthermal population from just above to just below the probe energy. Since more electrons will scatter to energies below the 270-meV probe than below the 220-meV one, the downward spike should be correspondingly stronger.

More intriguing, though, is that no spike is observed in ZrSiS—as evidenced by the lack of a negative transient at any pump energy, despite the material’s much lower  $E_F$ . Evidently, we never measure a non-thermal electronic distribution in ZrSiS, implying that electrons must thermalize efficiently within our time resolution—requiring rapid electron-electron ( $e-e$ ) scattering. The  $e-e$  scattering may be enhanced by ZrSiS’s low Fermi energy, which makes the  $e-e$  Coulomb interaction only weakly screened;<sup>37,38</sup> and also by the line node which, compared to point-node semimetals such as NbAs, provides a far larger density of states near  $E_F$ .

Our analyses of the spike and of the subsequent, slower relaxation rely heavily on our calculated  $\Delta R$ , so a few words about our model are in order. For the sake of broad applicability to Weyl and Dirac materials, we prioritized simplicity and independence from material parameters—such as the Fermi velocity and the number of nodes. Apart from  $E_F$ , the only material parameter used is the optical conductivity at the probe energy, which we obtain from infrared spectroscopy, described and shown in the [supplementary material](#).<sup>39–43</sup> In fact, writing  $\sigma = |\sigma|e^{i\theta}$ , only  $\theta$  influences our calculation, and not  $|\sigma|$ . For ZrSiS,  $\theta = 45^\circ$ ,<sup>44</sup> and for NbAs  $\theta = 21^\circ$  (see [supplementary material](#)). In the [supplementary material](#), we explore the effect of small differences in  $E_F$  and  $\theta$ .

We have treated  $\Delta\sigma$  as arising only from phase-space filling, leaving aside laser-induced modifications to the Drude conductivity, band renormalization, and saturation of the absorption. We treated the materials themselves as ideal: the densities of states  $g(E) \propto E$  and  $g(E) \propto E^2$  assume bands that disperse linearly, and are justified because both our pump and our probe energies lie within the Dirac and Weyl bands, so carriers are not excited in the massive bands at higher energy. Nonetheless, it is a radical simplification: it excludes particle-hole asymmetry, non-topological bands (though some are known to cross the Fermi energy of NbAs<sup>30,31</sup>) and curvature of the topological bands (which is known to occur around 100 meV in ZrSiS<sup>28,45</sup>). Despite these simplifications, our model finds applicability beyond our own experiment: the  $\Delta R(T_e)$  of Cd<sub>3</sub>As<sub>2</sub>, which Lu *et al.*<sup>24</sup> have inferred empirically, looks much like what we calculate

for NbAs. (Their sign differs, which happens for some values of  $\theta$ .)

We note, in closing, that previous experiments with 1.5-eV pump photons<sup>18,20–22,24</sup> have suggested picturing the ultrafast dynamics of topological semimetals as the cooling of hot Dirac or Weyl fermions. The simplicity of our experiment, in which both the pump and the probe lie within the topological bands, allows us to quantitatively validate this picture with a simple model for  $\Delta R$  vs.  $\Delta T_e$  that reproduces the principal features of  $\Delta R(t)$ , including its non-monotonic behavior and its different signs in ZrSiS and NbAs, without free parameters.

Additionally, we have demonstrated that Dirac and Weyl fermions may be directly excited. We have identified the signature of their initial, nonthermal distribution in a spike whose sign depends on the relative energy of the pump and the probe. Rapid  $e-e$  scattering depletes the nonthermal population, causing the Dirac or Weyl fermions to thermalize very quickly. Indeed, while the fastest transient in NbAs is thermalization, in ZrSiS, thermalization occurs within our time resolution, and the fastest transient is electronic cooling. Since this cooling controls the response-time of ultrafast devices, our result suggests that ZrSiS, in addition to being non-toxic and earth-abundant, may support even faster optical switches and detectors than does Cd<sub>3</sub>As<sub>2</sub>.<sup>12,16</sup>

See [supplementary material](#) for additional experimental details, analysis, and description of the model.

We acknowledge NSF DMR-1508278 and the Geoff and Josie Fox Scholarship. BVL acknowledges support by the Max Planck Society. Work at Princeton was supported by NSF through the Princeton Center for Complex Materials, a Materials Research Science and Engineering Center DMR-1420541, and by a MURI grant on Topological Insulators from the Army Research Office, ARO W911NF-12-1-0461. This research used resources of the Advanced Light Source, a DOE Office of Science User Facility under Contract No. DE-AC02-05CH11231.

<sup>1</sup>A. A. Burkov, M. D. Hook, and L. Balents, *Phys. Rev. B* **84**, 235126 (2011).

<sup>2</sup>X. Wan, A. M. Turner, A. Vishwanath, and S. Y. Savrasov, *Phys. Rev. B* **83**, 205101 (2011).

<sup>3</sup>S. M. Young, S. Zaheer, J. C. Y. Teo, C. L. Kane, E. J. Mele, and A. M. Rappe, *Phys. Rev. Lett.* **108**, 140405 (2012).

<sup>4</sup>H. Weng, C. Fang, Z. Fang, B. A. Bernevig, and X. Dai, *Phys. Rev. X* **5**, 011029 (2015).

<sup>5</sup>P. E. C. Ashby and J. P. Carbotte, *Phys. Rev. B* **89**, 245121 (2014).

<sup>6</sup>J. M. Shao and G. W. Yang, *AIP Adv.* **5**, 117213 (2015).

<sup>7</sup>Y. Baum, E. Berg, S. Parameswaran, and A. Stern, *Phys. Rev. X* **5**, 041046 (2015).

<sup>8</sup>O. V. Kotov and Y. E. Lozovik, *Phys. Rev. B* **93**, 235417 (2016).

<sup>9</sup>C.-K. Chan, N. H. Lindner, G. Refael, and P. A. Lee, *Phys. Rev. B* **95**, 041104 (2017).

<sup>10</sup>C. Triola, A. Pertsova, R. S. Markiewicz, and A. V. Balatsky, *Phys. Rev. B* **95**, 205410 (2017).

<sup>11</sup>S. Patankar, L. Wu, B. Lu, M. Rai, J. D. Tran, T. Morimoto, D. Parker, A. Grushin, N. L. Nair, J. G. Analytis, J. E. Moore, J. Orenstein, and D. H. Torchinsky, *Phys. Rev. B* **98**, 165113 (2018).

<sup>12</sup>Q. Wang, C.-Z. Li, S. Ge, J.-G. Li, W. Lu, J. Lai, X. Liu, J. Ma, D.-P. Yu, Z.-M. Liao, and D. Sun, *Nano Lett.* **17**, 834 (2017).

<sup>13</sup>N. Yavarishad, T. Hosseini, E. Kheirandish, C. P. Weber, and N. Kouklin, *Appl. Phys. Express* **10**, 052201 (2017).

<sup>14</sup>S. Chi, Z. Li, Y. Xie, Y. Zhao, Z. Wang, L. Li, H. Yu, G. Wang, H. Weng, H. Zhang, and J. Wang, preprint [arXiv:1705.05086](#) (2017).

- <sup>15</sup>M. Yang, J. Wang, J. Han, J. Ling, C. Ji, X. Kong, X. Liu, Z. Huang, J. Gou, Z. Liu, F. Xiu, and Y. Jiang, *ACS Photonics* **5**, 3438 (2018).
- <sup>16</sup>C. Zhu, F. Wang, Y. Meng, X. Yuan, F. Xiu, H. Luo, Y. Wang, J. Li, X. Lv, L. He, Y. Xu, Y. Shi, R. Zhang, and S. Zhu, *Nat. Commun.* **8**, 14111 (2017).
- <sup>17</sup>C. P. Weber, B. S. Berggren, M. G. Masten, T. C. Ogloza, S. Deckoff-Jones, J. Madéo, M. K. L. Man, K. M. Dani, L. Zhao, G. Chen, J. Liu, Z. Mao, L. M. Schoop, B. V. Lotsch, S. S. P. Parkin, and M. Ali, *J. Appl. Phys.* **122**, 223102 (2017).
- <sup>18</sup>C. Zhu, X. Yuan, F. Xiu, C. Zhang, Y. Xu, R. Zhang, Y. Shi, and F. Wang, *Appl. Phys. Lett.* **111**, 091101 (2017).
- <sup>19</sup>C. P. Weber, E. Arushanov, B. S. Berggren, T. Hosseini, N. Kouklin, and A. Nateprov, *Appl. Phys. Lett.* **106**, 231904 (2015).
- <sup>20</sup>Y. M. Dai, J. Bowlan, H. Li, H. Miao, S. F. Wu, W. D. Kong, Y. G. Shi, S. A. Trugman, J.-X. Zhu, H. Ding, A. J. Taylor, D. A. Yarotski, and R. P. Prasankumar, *Phys. Rev. B* **92**, 161104(R) (2015).
- <sup>21</sup>Y. Ishida, H. Masuda, H. Sakai, S. Ishiwata, and S. Shin, *Phys. Rev. B* **93**, 100302(R) (2016).
- <sup>22</sup>G. Wan, W. Yao, K. Zhang, C. Bao, C. Zhang, H. Zhang, Y. Wu, and S. Zhou, preprint [arXiv:1710.00350](https://arxiv.org/abs/1710.00350) (2017).
- <sup>23</sup>Y. M. Dai, B. Shen, L. X. Zhao, B. Xu, Y. K. Luo, A. P. Chen, R. Yang, X. G. Qiu, G. F. Chen, N. Ni, S. A. Trugman, J. X. Zhu, A. J. Taylor, D. A. Yarotski, and R. P. Prasankumar, in *2017 Conference on Lasers and Electro-Optics (CLEO)* (2017), pp. 1–2.
- <sup>24</sup>W. Lu, S. Ge, X. Liu, H. Lu, C. Li, J. Lai, C. Zhao, Z. Liao, S. Jia, and D. Sun, *Phys. Rev. B* **95**, 024303 (2017).
- <sup>25</sup>M. M. Jadidi, M. Mittendorff, S. Winnerl, B. Shen, A. B. Sushkov, G. S. Jenkins, N. Ni, H. D. Drew, and T. E. Murphy, in *Conference on Lasers and Electro-Optics* (Optical Society of America, 2017), p. FF1F.3.
- <sup>26</sup>G. Manzoni, A. Sterzi, A. Crepaldi, M. Diego, F. Cilento, M. Zacchigna, P. Bugnon, H. Berger, A. Magrez, M. Grioni, and F. Parmigiani, *Phys. Rev. Lett.* **115**, 207402 (2015).
- <sup>27</sup>L. M. Schoop, M. N. Ali, C. Straßer, T. Andreas, V. Andrei, D. Marchenko, V. Duppel, S. S. Parkin, B. V. Lotsch, and C. R. Ast, *Nat. Commun.* **7**, 11696 (2016).
- <sup>28</sup>M. B. Schilling, L. M. Schoop, B. V. Lotsch, M. Dressel, and A. V. Pronin, *Phys. Rev. Lett.* **119**, 187401 (2017).
- <sup>29</sup>S.-Y. Xu, N. Alidoust, I. Belopolski, Z. Yuan, G. Bian, T.-R. Chang, H. Zheng, V. N. Strocov, D. S. Sanchez, G. Chang, C. Zhang, D. Mou, Y. Wu, L. Huang, C.-C. Lee, S.-M. Huang, B. Wang, A. Bansil, H.-T. Jeng, T. Neupert, A. Kaminski, H. Lin, S. Jia, and M. Zahid Hasan, *Nat. Phys.* **11**, 748 (2015).
- <sup>30</sup>Y. Luo, N. J. Ghimire, E. D. Bauer, J. D. Thompson, and F. Ronning, *J. Phys.: Condens. Matter* **28**, 055502 (2016).
- <sup>31</sup>R. Singha, A. K. Pariari, B. Satpati, and P. Mandal, *Proc. Natl. Acad. Sci.* **114**, 2468–2473 (2017).
- <sup>32</sup>J. Y. Liu, J. Hu, Q. Zhang, D. Graf, H. B. Cao, S. M. A. Radmanesh, D. J. Adams, Y. L. Zhu, G. F. Cheng, X. Liu, W. A. Phelan, J. Wei, M. Jaime, F. Balakirev, D. A. Tennant, J. F. DiTusa, I. Chiorescu, L. Spinu, and Z. Q. Mao, *Nat. Mater.* **16**, 905 (2017).
- <sup>33</sup>S. V. Ramankutty, J. Henke, A. Schiphorst, R. Nutakki, S. Bron, G. Araizi-Kanoutas, S. K. Mishra, L. Li, Y. K. Huang, T. K. Kim, M. Hoesch, C. Schlueter, T.-L. Lee, A. de Visser, Z. Zhong, J. van Wezel, E. van Heumen, and M. S. Golden, *SciPost Phys.* **4**, 010 (2018).
- <sup>34</sup>W. Pötz and P. Kocevar, *Phys. Rev. B* **28**, 7040 (1983).
- <sup>35</sup>W. Zhou, H. Gao, J. Zhang, R. Fang, H. Song, T. Hu, A. Stroppa, L. Li, X. Wang, S. Ruan, and W. Ren, *Phys. Rev. B* **96**, 064103 (2017).
- <sup>36</sup>M. V. Lebedev, O. V. Misochko, T. Dekorsy, and N. Georgiev, *J. Exp. Theor. Phys.* **100**, 272 (2005).
- <sup>37</sup>Y. Huh, E.-G. Moon, and Y. B. Kim, *Phys. Rev. B* **93**, 035138 (2016).
- <sup>38</sup>S. Pezzini, M. R. van Delft, L. M. Schoop, B. V. Lotsch, A. Carrington, M. I. Katsnelson, N. E. Hussey, and S. Wiedmann, *Nat. Phys.* **14**, 178 (2017).
- <sup>39</sup>A. B. Kuzmenko, *Rev. Sci. Instrum.* **76**, 083108 (2005).
- <sup>40</sup>S.-i. Kimura, H. Yokoyama, H. Watanabe, J. Sichelschmidt, V. Süß, M. Schmidt, and C. Felser, *Phys. Rev. B* **96**, 075119 (2017).
- <sup>41</sup>D. B. Tanner, *Phys. Rev. B* **91**, 035123 (2015).
- <sup>42</sup>B. L. Henke, E. M. Gullikson, and J. C. Davis, *At. Data Nucl. Data Tables* **54**, 181 (1993).
- <sup>43</sup>See [http://henke.lbl.gov/optical\\_constants/](http://henke.lbl.gov/optical_constants/) for X-ray atomic scattering functions.
- <sup>44</sup>A. V. Pronin, private communication (23 July 2018).
- <sup>45</sup>T. Habe and M. Koshino, *Phys. Rev. B* **98**, 125201 (2018).